

## Dynamical Balances and Tropical Stratospheric Upwelling

WILLIAM J. RANDEL, ROLANDO GARCIA, AND FEI WU

*National Center for Atmospheric Research,\* Boulder, Colorado*

(Manuscript received 4 February 2008, in final form 17 April 2008)

### ABSTRACT

The dynamical balances associated with upwelling in the tropical lower stratosphere are investigated based on climatological 40-yr ECMWF Re-Analysis (ERA-40) and NCEP–NCAR reanalysis data. Zonal mean upwelling is calculated from momentum balance and continuity (“downward control”), and these estimates in the deep tropics are found to be in reasonable agreement with stratospheric upwelling calculated from thermodynamic balance (and also with vertical velocity obtained from ERA-40). The detailed momentum balances associated with the dynamical upwelling are investigated, particularly the contributions to climatological Eliassen–Palm (EP) flux divergence in the subtropics. Results show that the equatorward extension of extratropical waves (baroclinic eddies and, in the NH, quasi-stationary planetary waves) contribute a large component of the subtropical wave driving at 100 hPa. Additionally, there is a significant contribution to subtropical forcing from equatorial planetary waves, which exhibit a strong seasonal cycle (a reversal in phase) in response to latitudinal migration of tropical convection. The observed balances suggest that the strong annual cycle in upwelling across the tropical tropopause is forced by subtropical horizontal eddy momentum flux convergence associated with waves originating in both the tropics and extratropics.

### 1. Introduction

The general circulation of the stratosphere is characterized by a global overturning circulation with upwelling in the tropics and poleward–downward flow in the extratropics. This so-called Brewer–Dobson circulation was postulated based on observations of stratospheric water vapor (Brewer 1949) and ozone (Dobson 1956) and later confirmed from calculations of diabatic circulations in the stratosphere (e.g., Murgatroyd and Singleton 1961; Gille et al. 1987). This overturning circulation is fundamentally driven by waves that propagate from a variety of sources in the troposphere to the stratosphere, producing a transport of angular momentum and resulting in balanced poleward mass flux in the stratosphere (Haynes et al. 1991; Holton et al. 1995). The induced upwelling in the tropics maintains temperatures below radiative equilibrium (which are balanced by radiative heating), with corresponding down-

welling, dynamical heating, and radiative cooling at high latitudes. The tropical upwelling is a key feature of stratosphere–troposphere coupling; air enters the stratosphere primarily in the tropics, and the chemical composition of air near the tropical tropopause sets the boundary condition for the composition of the global stratosphere. Although the tropical upwelling is a key feature of the stratospheric circulation, it has a small magnitude ( $\sim 0.05 \text{ mm s}^{-1}$  or  $\sim 8 \text{ km yr}^{-1}$ ) that cannot be measured directly; the strength of upwelling is typically inferred from thermodynamic balance (e.g., Rosenlof 1995) or from observations of trace constituents (e.g., Hall and Waugh 1997; Mote et al. 1998; Niwano et al. 2003).

A further key aspect of the tropical upwelling is that there is a relatively large annual cycle in the lower stratosphere, with strongest upwelling during NH winter. This seasonality is reflected in a large annual cycle in temperature near and above the tropopause (Reed and Vlcek 1969), which in turn imparts a seasonal cycle to stratospheric water vapor (Mote et al. 1996). This seasonal cycle in upwelling is also reflected in chemical constituents with a strong vertical gradient in the tropical lower stratosphere, such as ozone and carbon monoxide (Randel et al. 2007). Yulaeva et al. (1994) suggested that this seasonal cycle in tropical upwelling

---

\* The National Center for Atmospheric Research is sponsored by the National Science Foundation.

---

*Corresponding author address:* William J. Randel, NCAR, P.O. Box 3000, Boulder, CO 80307–3000.  
E-mail: randel@ucar.edu

could result from extratropical planetary wave forcing of the stratosphere; the maximum in wave forcing occurs during September–November in the SH and November–March in the NH, so that there is a global forcing with maximum during NH winter. However, as discussed by Plumb and Eluszkiewicz (1999), the wave forcing [or Eliassen–Palm (EP) flux divergence] required to drive near-equatorial upwelling must extend to very low latitudes, so the role of extratropical planetary waves is uncertain. More recently, Boehm and Lee (2003), Kerr-Munslow and Norton (2006), and Norton (2006) have proposed that upwelling is linked to equatorial planetary waves forced by tropical deep convection. Overall, the specific forcing of tropical stratospheric upwelling and the cause of the large annual cycle are poorly understood. The forcing of the Brewer–Dobson circulation has also received recent attention because model simulations of future climate change associated with greenhouse gas increases show persistent increases in the strength of the circulation (Butchart et al. 2006; Fomichev et al. 2007; Garcia and Randel 2008).

The objective of this paper is to examine tropical upwelling derived from momentum balance [the so-called “downward control” of Haynes et al. (1991)] to understand mechanisms that maintain the upwelling. Calculations are based on climatological circulation statistics derived from reanalysis datasets. We first make detailed comparisons between upwelling calculated from momentum balance with results from thermodynamic balance (and also with upwelling derived directly from reanalyses); these comparisons suggest that momentum balance provides a reasonable estimate of the space–time behavior of climatological upwelling in the deep tropics near and above the tropopause. We then examine the detailed structure of the momentum balance, and in particular we focus on the wave forcing in the subtropics responsible for the near-equatorial upwelling.

## 2. Data and tropical upwelling calculations

The circulation statistics used here are based on global meteorological reanalysis datasets from the 40-yr European Centre for Medium-Range Weather Forecasts (ECMWF) Re-Analysis (ERA-40; Uppala et al. 2005) and from the National Centers for Environmental Prediction–National Center for Atmospheric Research

(NCEP–NCAR; Kalnay et al. 1996). We use the ERA-40 data archived on 60 vertical pressure levels, with a vertical resolution of  $\sim 0.8$  km in the upper troposphere–lower stratosphere (UTLS) region. The NCEP calculations use data on 23 standard pressure levels, with somewhat lower vertical resolution ( $\sim 2$  km) in the UTLS region. The latitude resolution of both datasets is  $2.5^\circ$ . We have derived monthly averaged statistics from daily analysis, and the results here are based on averages over 1994–2001. We use the pressure velocity ( $\omega$ ) converted to log-pressure vertical velocity ( $w$ ) and note that for NCEP reanalysis the uppermost output level for the vertical velocity is 100 hPa (values are zero above this level). Comparisons of the zonal mean vertical velocity  $\bar{w}$  show a reasonable behavior for the ERA-40 data throughout the UTLS (as shown below), whereas the NCEP results show an unrealistic seasonal cycle at 100 hPa (minimum during NH winter). We thus focus primarily on the ERA-40  $\bar{w}$  values. We also calculate zonal average eddy covariance statistics from both ERA-40 and NCEP data, including  $\overline{v'T'}$ ,  $\overline{u'v'}$ , and  $\overline{u'w'}$  (throughout this work notation is standard, following Andrews et al. 1987). Note that for NCEP data,  $\overline{u'w'}$  is identically zero above 100 hPa.

We calculate the zonal average transformed Eulerian mean (TEM) residual vertical velocity from the ERA-40 data from

$$\overline{w^*} = \bar{w} + \frac{1}{a \cos \phi} \frac{\partial}{\partial \phi} \left( \cos \phi \frac{\overline{v'T'}}{S} \right). \quad (1)$$

Here  $S$  is a static stability term:  $S = HN^2/R$ , with  $H = 7$  km and  $R = 287 \text{ m}^2 \text{ s}^{-2} \text{ K}^{-1}$ , and  $N^2$  is the Brunt–Väisälä frequency squared. In the deep tropics, the eddy term in (1) makes only a small contribution, so that  $\overline{w^*} \approx \bar{w}$ . It is worthwhile noting that  $\bar{w}$  derived from reanalyses can have substantial uncertainties in the UTLS region because it is a quantity that is poorly constrained in current data assimilation products. Hence, we do not view the ERA-40  $\overline{w^*}$  fields as “truth,” but rather as simply another estimate to compare to the dynamic and thermodynamic balance results.

We estimate tropical upwelling from the TEM zonal average momentum balance and continuity, following the calculations discussed in Haynes et al. (1991) and Randel et al. (2002). Specifically, the zonal average vertical velocity at altitude  $z$ , averaged between latitudes  $\phi_1$  and  $\phi_2$ , is given by [Randel et al. 2002, their Eq. (11)]

$$\langle \overline{w_m^*} \rangle(z) = \frac{e^{z/H}}{\int_{\phi_1}^{\phi_2} a \cos \phi d\phi} \left\{ -\cos \phi \int_z^\infty \frac{[DF(\phi, z') - \bar{u}_t(\phi, z')]}{\hat{f}(\phi, z')} e^{-z'/H} dz' \right\}_{\phi_1}^{\phi_2}. \quad (2)$$

Here the subscript  $m$  denotes vertical velocity derived from momentum balance, and angle brackets denote an average between latitudes  $\phi_1$  and  $\phi_2$ ; note that this equation includes the time tendency of the zonal mean zonal wind as a generalization of the Haynes et al. (1991) steady state calculation. Also,  $\hat{f}$  is a modified Coriolis parameter,  $\hat{f} = f - (1/a \cos\phi)(\partial/\partial\phi)(\bar{u} \cos\phi)$ ; DF is the scaled EP flux divergence,

$$\text{DF} = \frac{e^{z/H}}{a \cos\phi} \nabla \cdot \mathbf{F}, \quad (3)$$

where  $\mathbf{F}$  is the EP flux vector:

$$F_\phi = e^{-z/H} a \cos\left[ -\overline{u'v'} + \left( \frac{\partial \bar{u}}{\partial z} \right) \frac{\overline{v'T'}}{S} \right] \quad (4a)$$

$$F_z = e^{-z/H} a \cos\phi \left( \hat{f} \frac{\overline{v'T'}}{S} + \overline{u'w'} \right). \quad (4b)$$

We note that the  $\langle \overline{w_m^*} \rangle$  estimates from (2) become problematic close to the equator because of uncertainties associated with estimating the EP flux divergence combined with an overall proportionality to  $1/\hat{f}$ . We find that the climatological calculations are reasonably well behaved for latitudes  $\geq 15^\circ\text{N}$  and  $^\circ\text{S}$ . Below we separate the contributions to  $\langle \overline{w_m^*} \rangle$  in the tropics from the separate terms in the vertical integral in (2), that is, the components of DF ( $\overline{u'v'}$ ,  $\overline{v'T'}$ , etc.) and  $\bar{u}_r$ .

Another method of estimating the mean tropical upwelling is based on the quasigeostrophic TEM thermodynamic equation

$$\frac{\partial \bar{T}}{\partial t} + \bar{v}^* \frac{\partial \bar{T}}{\partial y} + \bar{w}^* S = \bar{Q}, \quad (5)$$

where  $\bar{Q}$  is the zonal average radiative heating rate, combined with the continuity equation (e.g., Gille et al. 1987; Rosenlof 1995). These equations are solved iteratively, and the resulting vertical velocity is termed  $\bar{w}_Q^*$  because it is derived primarily from radiative heating calculations. We calculate  $\bar{Q}$  based on an accurate radiative heating code (Qiang Fu 2005, personal communication), incorporating monthly varying temperatures and radiatively relevant trace species (including realistic variations of stratospheric ozone and water vapor). The temperature climatology is derived from several years of GPS radio occultation data (e.g., Wickert et al. 2001; Randel et al. 2003), which provides high vertical resolution and accurately captures the cold tropical tropopause region. The calculations of  $\bar{w}_Q^*$  are mainly valid at and above 100 hPa, where radiation dominates the thermodynamic forcing. The radiative calculations do not include effects of thin cirrus near the tropopause, but these probably do not strongly influence the zonal mean results (Corti et al. 2006; Fueglistaler and Fu 2006). The inclusion of tropospheric clouds may also

decrease the radiatively derived upwelling above the lower stratosphere (Yang et al. 2008), but the focus here is on the UTLS region.

We also use outgoing longwave radiation (OLR) data as a proxy for tropical deep convection (and associated convective heat release). Daily interpolated OLR data are obtained by the National Oceanic and Atmospheric Administration–Cooperative Institute for Research in Environmental Sciences (NOAA–CIRES) Climate Diagnostics Center (<http://www.cdc.noaa.gov>). These data are discussed in detail in Liebmann and Smith (1996). The climatological results shown here are averages over the years 1994–2001 (identical to the circulation statistics).

### 3. Results

#### a. Comparison of different upwelling estimates

The latitude–month variation of zonal average velocity at 100 hPa derived from  $\bar{w}_Q^*$  is shown in Fig. 1a, together with the ERA-40  $\bar{w}^*$  in Fig. 1b. The structure of  $\bar{w}_Q^*$  is reasonably smooth, with tropical upwelling shifted slightly toward the summer hemisphere (this shift is more pronounced at higher altitudes). These results are similar to the calculations of Rosenlof (1995) and Eluszkiewicz et al. (1996). There is a clear seasonal cycle in the tropics, with strongest upwelling during NH winter (in balance with the seasonal cycle in tropical temperatures; cf. Yulaeva et al. 1994). The ERA-40  $\bar{w}^*$  data (Fig. 1b) show similar overall patterns and magnitudes, but there is substantially more small-scale meridional structure in the data assimilation result. As noted above, the eddy term in (1) makes only a small contribution in the tropics, so the small-scale meridional structure seen in Fig. 1b is primarily due to the  $\bar{w}$  field in ERA-40.

Figure 2a compares the 100-hPa vertical velocity estimates averaged over the tropical latitude band  $15^\circ\text{N}$ – $15^\circ\text{S}$ , including  $\langle \overline{w^*} \rangle$  from ERA-40 and  $\langle \bar{w}_Q^* \rangle$  and  $\langle \overline{w_m^*} \rangle$  from both ERA-40 and NCEP. Overall there is reasonable agreement among the estimates, in particular for the magnitude of upwelling and the structure of the seasonal cycle (the strongest upwelling occurs during NH winter). The NCEP  $\langle \overline{w_m^*} \rangle$  exhibits a larger-amplitude seasonal cycle than the other estimates, with notably smaller values during NH summer, although as shown below this difference may simply reflect the lack of a realistic  $\overline{u'w'}$  contribution in NCEP data (due to the absence of vertical velocity fields above 100 hPa). Figure 2b shows a similar comparison for a wider latitude band ( $25^\circ\text{N}$ – $25^\circ\text{S}$ ); in this case, the values of  $\langle \overline{w_m^*} \rangle$  estimated from both ERA-40 and NCEP data agree reasonably well, but they are systematically smaller

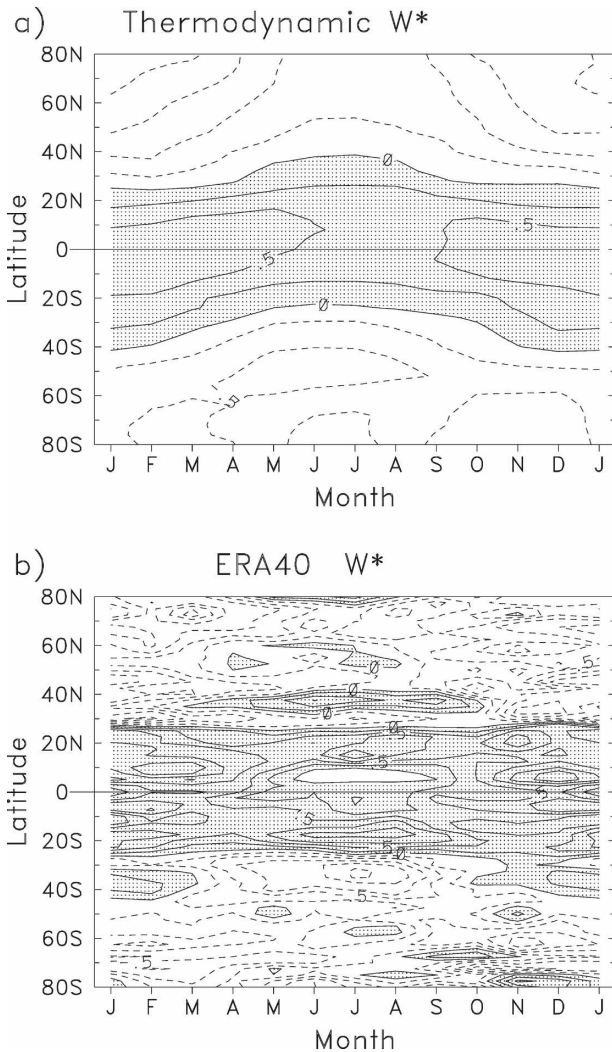


FIG. 1. Latitude–month diagrams of climatological zonal mean residual vertical velocity at 100 hPa, (a) based on thermodynamic calculations  $\overline{w}_Q^*$  and (b) derived from ERA-40 reanalysis  $\overline{w}^*$ . Contour interval is  $0.25 \text{ mm s}^{-1}$ , with positive (upward) values shaded.

than and exhibit a seasonal phase shift compared to  $\langle \overline{w}^* \rangle$  and  $\langle \overline{w}_Q^* \rangle$ . These systematic differences may suggest some unresolved eddy momentum forcing in the reanalysis datasets, such as could result from subtropical gravity wave drag (as discussed further below). At higher altitudes in the lower stratosphere (e.g., 70 and 50 hPa), comparisons similar to those in Fig. 2 show somewhat less agreement than the results at 100 hPa, with the calculated  $\langle \overline{w}_m^* \rangle$  from both ERA-40 and NCEP data showing approximately half the magnitude of  $\langle \overline{w}_Q^* \rangle$ ; the ERA-40  $\langle \overline{w}^* \rangle$  also becomes unrealistic at higher altitudes, with a incorrect seasonal cycle (maximum during NH summer) near 50 hPa.

The latitudinal structure of vertical velocity at 100 hPa for each of the estimates is shown in Fig. 3, includ-

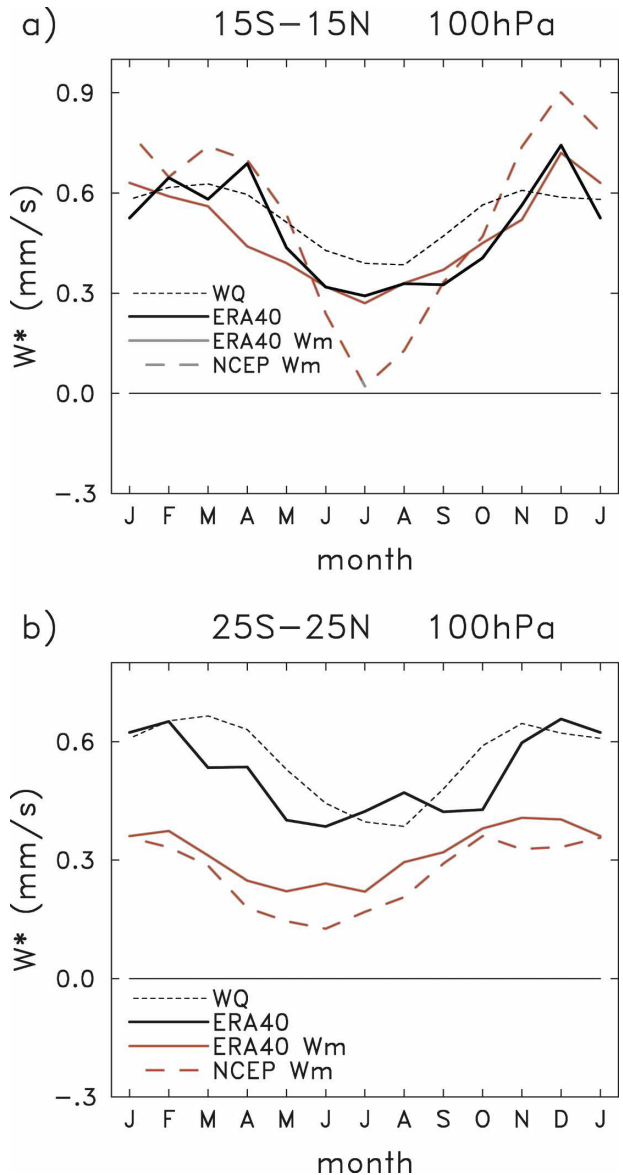


FIG. 2. Seasonal cycle of zonal mean upwelling at 100 hPa, based on ERA-40 and thermodynamic and momentum balance as noted. Results are shown for averages over latitudes (a)  $15^\circ\text{N}$ – $15^\circ\text{S}$  and (b)  $25^\circ\text{N}$ – $25^\circ\text{S}$ .

ing the annual mean (Fig. 3a) and the December–February (DJF; Fig. 3b) and June–August (JJA) seasons (Fig. 3c). Here the  $\langle \overline{w}_m^* \rangle$  estimates are calculated for the latitude band  $15^\circ\text{N}$ – $15^\circ\text{S}$  [because the estimates from (2) are poorly behaved equatorward of  $15^\circ$ ] and for each individual  $5^\circ$  latitude band poleward of  $15^\circ$ . Figure 3a shows good agreement between the  $\overline{w}^*$ ,  $\overline{w}_Q^*$ , and  $\langle \overline{w}_m^* \rangle$  estimates close to the equator (consistent with Fig. 2a). However, there are some substantial differences in the latitude range  $\sim 15^\circ$ – $25^\circ$  in both hemispheres, where the assimilation result  $\overline{w}^*$  shows a maxi-

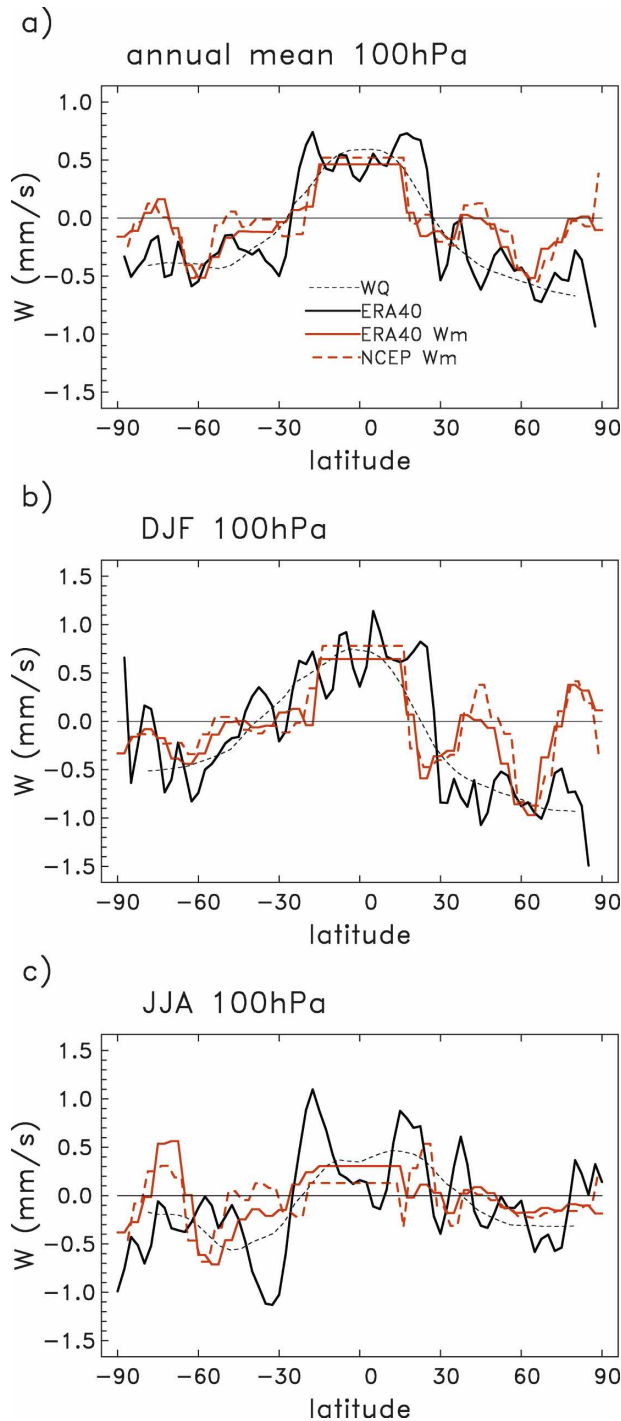


FIG. 3. Latitudinal structure of zonal mean residual vertical velocity at 100 hPa, based on ERA-40 and thermodynamic and momentum balance estimates: (a) annual mean; (b), (c) seasonal estimates for DJF and JJA, respectively.

mum,  $\bar{w}_m^*$  exhibits near-zero values, and  $\bar{w}_Q^*$  displays values in between; this is the source of the systematic differences seen in Fig. 2b. Poleward of  $\sim 30^\circ$ , each of the vertical velocity estimates in Fig. 3a shows predomi-

nant downwelling, although with substantially different detailed structures.

The seasonal upwelling comparisons in Figs. 3b,c show more substantial differences in detail among the different upwelling estimates. The slight latitudinal movement of the tropical maximum in  $\bar{w}_Q^*$  toward the summer hemisphere is not evident in  $\bar{w}^*$  or  $\bar{w}_m^*$ , and there are large latitudinal variations in  $\bar{w}^*$  and  $\bar{w}_m^*$  that are absent in  $\bar{w}_Q^*$ . Nonetheless, when averaged over the deep tropics ( $15^\circ\text{N}$ – $15^\circ\text{S}$ ), there is at least some agreement in upwelling magnitudes, with larger values during DJF than during JJA (cf. Fig. 2).

The systematic differences in  $\bar{w}^*$  over  $15$ – $25^\circ\text{N}$  and  $^\circ\text{S}$  in Fig. 3 could be suggestive of some unresolved eddy momentum forcing in the reanalysis data, such as might result from gravity wave drag atop the subtropical jets (McFarlane 1987). We have tested this hypothesis using output from the NCAR Whole Atmosphere Community Climate Model (WACCM; Garcia et al. 2007), which includes both the large-scale circulation (as resolved using a  $1.9^\circ \times 2.5^\circ$  horizontal grid) and a gravity wave parameterization (including both orographic and nonorographic wave sources); the dynamical climatology of this model is described in detail in Richter et al. (2008). Briefly, we have performed calculations identical to the observational analyses discussed above, comparing  $\bar{w}^*$  from the model with  $\bar{w}_m^*$  estimated from the resolved eddies and also with  $\bar{w}_m^*$  calculations including the parameterized gravity wave drag. Figure 4a shows a comparison of the calculations based on including just the resolved waves at 100 hPa (for annual average results). There is overall agreement for the broadest-scale features, but substantial disagreement in the detailed latitudinal structures; overall, these results look similar to the observational analyses in Fig. 3a. Figure 4b shows a similar calculation, but in this case the gravity wave drag estimated in the model is included as a forcing term in Eq. (2) as an additional term in DF. In the model there is maximum gravity wave drag on top of the subtropical jets, especially in the NH (associated with orographically generated waves). The results in Fig. 4b show much better agreement in detail between  $\bar{w}^*$  and  $\bar{w}_m^*$  than in Fig. 4a, in particular for the NH where the modeled gravity drag is largest. These comparisons demonstrate the importance of gravity wave drag for tropical stratospheric upwelling (especially in the subtropics) in the context of a global circulation model. By analogy, the relatively large differences in the subtropics seen in the observational analyses (Figs. 2b and 3) may be associated with the neglect of gravity wave drag near the top of the subtropical jets (which is unresolved in the reanalysis data).

Figure 5 compares the vertical structures of annual

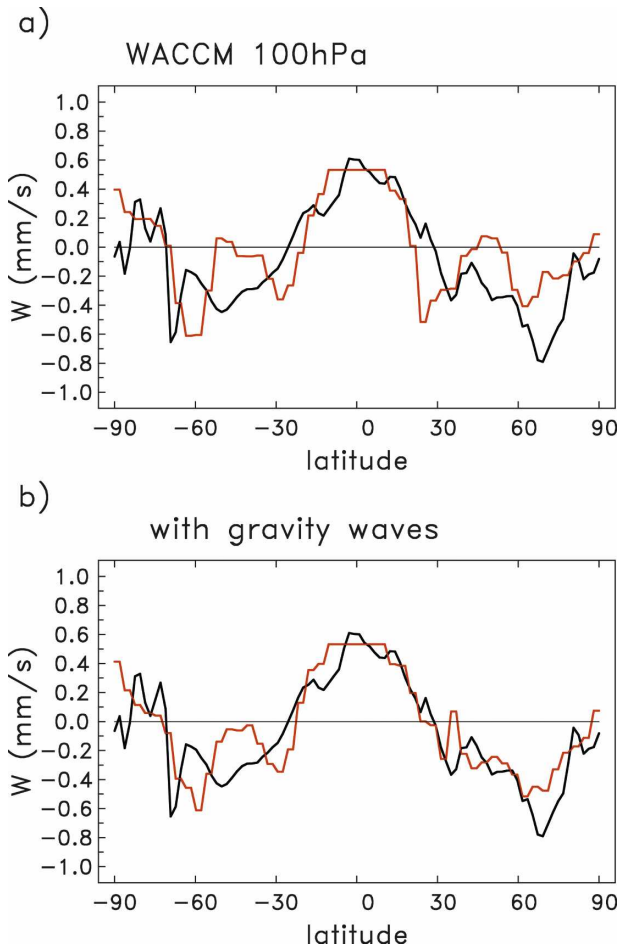


FIG. 4. Latitudinal structure of annual average 100-hPa zonal mean residual vertical velocity derived from WACCM model output (black lines), compared with momentum balance estimates (red lines): (a) momentum balance derived from the resolved eddies; (b) results including parameterized gravity wave drag. Black lines are identical in (a) and (b).

mean upwelling over 15°N–15°S, for pressure levels 200–50 hPa (~11–21 km); note that the  $\langle \bar{w}_Q^* \rangle$  radiative estimate is only calculated at and above 100 hPa. Overall there is reasonable agreement between  $\langle \bar{w}_m^* \rangle$  and  $\langle \bar{w}^* \rangle$  below ~70 hPa, whereas above this level  $\langle \bar{w}^* \rangle$  is somewhat larger than both  $\langle \bar{w}_m^* \rangle$  and  $\langle \bar{w}_Q^* \rangle$ ;  $\langle \bar{w}_m^* \rangle$  shows good agreement with  $\langle \bar{w}_Q^* \rangle$  at 100 hPa, but decreases faster with altitude above this level. Overall, for the deep tropics (15°N–15°S) and altitudes spanning the UTLS (~11–18 km), values of  $\langle \bar{w}_m^* \rangle$  estimated using circulation statistics from both ERA-40 and NCEP exhibit a seasonal cycle and vertical structure consistent with the other upwelling estimates. This is a key point because the detailed structure of the momentum balance can then be analyzed to understand the forcing of  $\langle \bar{w}_m^* \rangle$ .

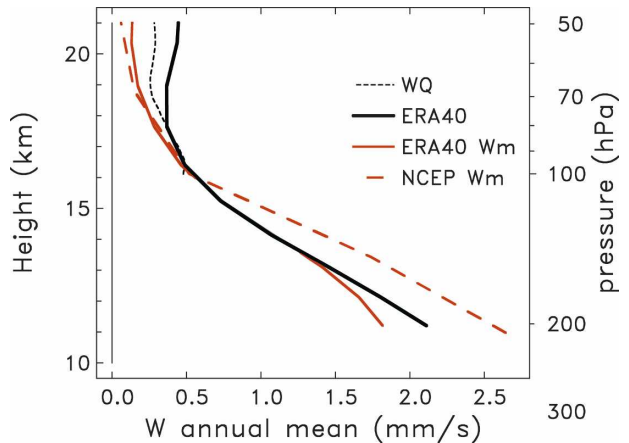


FIG. 5. Vertical structure of the annual mean zonal mean vertical velocity averaged over 15°N–15°S, based on ERA-40 reanalysis and thermodynamic and momentum balance estimates. The thermodynamic estimate is only calculated at and above 100 hPa.

*b. Contributions to momentum balance upwelling*

In this section we analyze the different contributions to  $\langle \bar{w}_m^* \rangle$  by focusing on the individual terms in the vertical integral in (2); that is, we consider the separate eddy forcing contributions to DF (and also the contribution of  $\bar{u}_r$ ). Figure 6 shows the seasonal variation of 100 hPa  $\langle \bar{w}_m^* \rangle$  for 15°N–15°S for both ERA-40 and NCEP data (the same curves as included in Fig. 2), together with the individual contributions from the components of DF and  $\bar{u}_r$ . There are four separate terms in DF, proportional to the quantities  $(\partial/\partial\phi)u'v'$ ,  $(\partial/\partial\phi)((\partial\bar{u}/\partial z)v'T')$ ,  $(\partial/\partial z)(v'T')$ , and  $(\partial/\partial z)(u'w')$ . Figure 6 shows that the dominant term in  $\langle \bar{w}_m^* \rangle$  is the meridional momentum flux convergence term  $(\partial/\partial\phi)u'v'$ , and that this term also accounts for almost all of the seasonal variation in  $\langle \bar{w}_m^* \rangle$ . The other terms in DF make relatively small contributions during the NH winter, whereas several terms contribute small components during NH summer (when the net upwelling is weak). The overall balance among terms is quite consistent between the ERA-40 and NCEP results, and the only substantial difference is in the  $(\partial/\partial z)(u'w')$  term (which is unreliable in the NCEP data because  $u'w'$  is identically zero above 100 hPa, as noted above). As a note, we find that the balance of terms contributing to upwelling over 15°N–15°S in the WACCM model (discussed above) is very similar to the balances shown in Fig. 6. We also note that although Kerr-Munslow and Norton (2006) find a dominant contribution to upwelling from the  $(\partial/\partial z)(u'w')$  term based on ERA-15 reanalysis, that result is not confirmed in the ERA-40 results here.

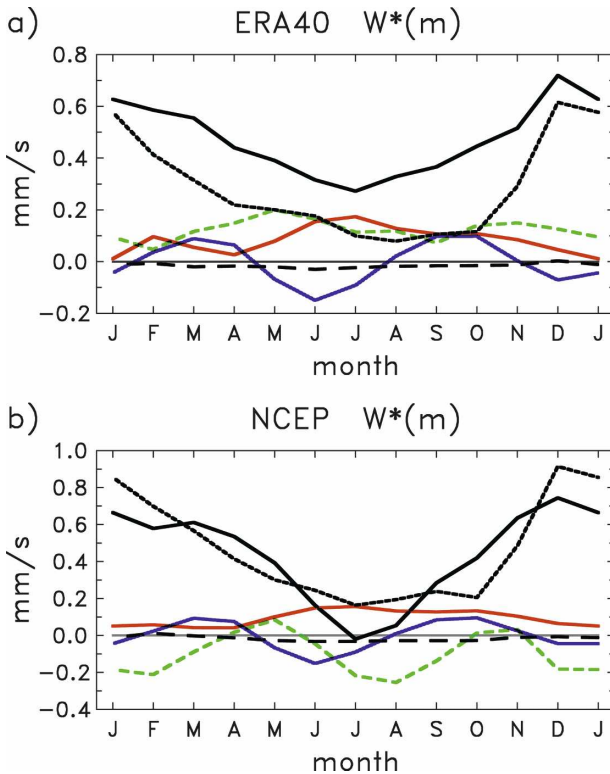


FIG. 6. Seasonal cycle of momentum balance upwelling over  $15^\circ\text{N}$ – $15^\circ\text{S}$  at 100 hPa (heavy solid lines), together with the individual terms contributing to the forcing from Eq. (2). The separate lines correspond to  $(\partial/\partial\phi)(\bar{u}'v')$  (black short dashed),  $(\partial/\partial z)(\bar{v}'T')$  (red),  $(\partial/\partial z)(\bar{u}'w')$  (green),  $(\partial/\partial\phi)((\partial\bar{u}/\partial z)\bar{v}'T')$  (black long dashed), and  $\bar{u}_r$  (blue). Results are shown based on (a) ERA-40 and (b) NCEP data.

The structure of the climatological EP flux divergence associated with the tropical upwelling is analyzed further in Fig. 7, which shows an EP flux diagram for annual average statistics derived from ERA-40 data. This diagram shows  $\mathbf{F}$  as a vector field (representing wave activity flux), superimposed on contours of DF, and we have used a latitude axis proportional to  $\sin\phi$  to accentuate the tropics and a vertical domain of 5–20 km to highlight the UTLS region. Figure 7 shows the well-known climatological structure of EP flux with upward and equatorward pointing arrows in the extratropics of both hemispheres, which are primarily associated with midlatitude baroclinic eddies, and also quasi-stationary planetary waves during NH winter (Edmon et al. 1980). The horizontal turning of the arrows in the upper troposphere and equatorward extension of the overall patterns is associated with equatorward propagation of wave activity flux, and there is a strong convergence of EP flux in the subtropical upper troposphere of both hemispheres (extending over  $\sim 10^\circ$ – $30^\circ$ ). The EP flux convergence at subtropical latitudes, which extends

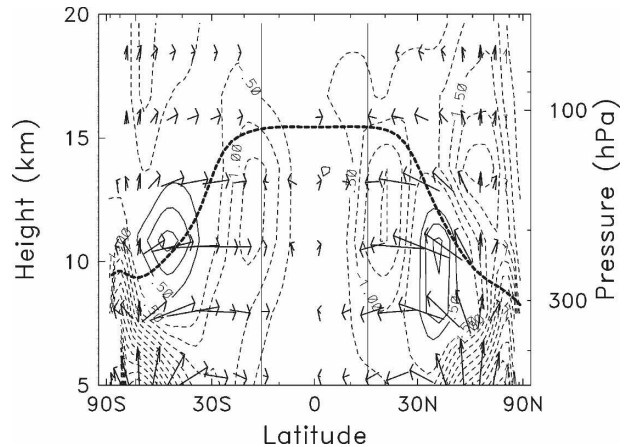


FIG. 7. Annual average EP flux diagram derived from ERA-40 data. Contours show the wave driving DF, with a contour interval of  $0.5 \text{ m s}^{-1} \text{ day}^{-1}$  (zero contours omitted). The latitude axis is proportional to  $\sin(\text{latitude})$  to accentuate tropical latitudes. The heavy dashed line denotes the time-averaged tropopause, and the vertical lines at  $15^\circ\text{N}$ – $15^\circ\text{S}$  denote the limits for  $(\bar{w}_m^*)$  calculations.

across the 100-hPa level, is in balance with upwelling across the tropical tropopause. Note that the fact that the meridional momentum flux convergence  $(\partial/\partial\phi)\bar{u}'v'$  is a dominant contribution in Fig. 6 is consistent with the predominantly horizontal EP flux vector impinging on the subtropics in Fig. 7.

A key aspect of the tropical upwelling is the large seasonal cycle, and the EP flux patterns associated with the seasonal extremes (DJF and JJA) are shown in Figs. 8a,b. These patterns show stronger EP flux divergence in the subtropics of the respective winter hemispheres, and inspection of the EP flux vectors shows that this occurs because of two distinct regions of wave activity flux. First, there is the equatorward propagation of extratropical wave activity, which is somewhat stronger in the winter as compared to the summer hemispheres. Second, there is significant wave activity flux in the tropics between  $15^\circ\text{N}$  and  $15^\circ\text{S}$ , which points northward in DJF and southward in JJA; note that the EP flux vectors show a clear distinction between the direction of tropical versus extratropical wave activity flux. The combination of the extratropical and equatorial wave fluxes results in strong EP flux convergence over  $\sim 10^\circ$ – $25^\circ\text{N}$  in DJF and  $\sim 10^\circ$ – $25^\circ\text{S}$  in JJA. The seasonally varying tropical wave fluxes are associated with equatorial planetary waves forced by persistent tropical convection (Gill 1980; Norton 2006; Dima et al. 2005; Dima and Wallace 2007). Figure 9 shows the spatial structure of the climatological tropical waves (geopotential height and winds at 200 hPa) from ERA-40 data, together with outgoing longwave radiation (a proxy for deep convection) for DJF and JJA; these are

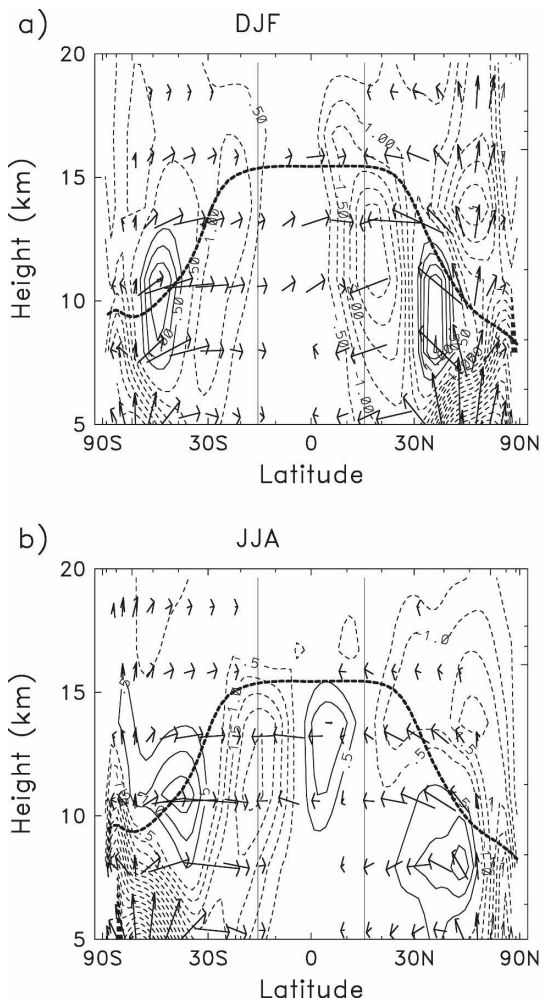


FIG. 8. Seasonal average EP flux diagrams calculated from ERA-40 data with results for (a) DJF and (b) JJA. Details are the same as in Fig. 7.

similar to results using NCEP data shown in Dima et al. 2005. The regions of strongest convection in the western Pacific (DJF) and within the Asian summer monsoon system (JJA) are associated with equatorial planetary waves, and part of the wave structure includes winds producing southward (DJF) and northward (JJA) momentum fluxes (which balance the Coriolis acceleration associated with the local Hadley circulation, as discussed in Dima et al. 2005). The equatorial wave momentum flux patterns change sign between DJF and JJA in response to the movement of convection to the respective summer hemisphere. These equatorial wave fluxes are an important contribution to the subtropical EP flux convergences seen in Figs. 8a,b, and hence to tropical  $\langle \bar{w}_m^* \rangle$ .

One further aspect of note in Figs. 8a,b is that the subtropical EP fluxes during DJF extend somewhat

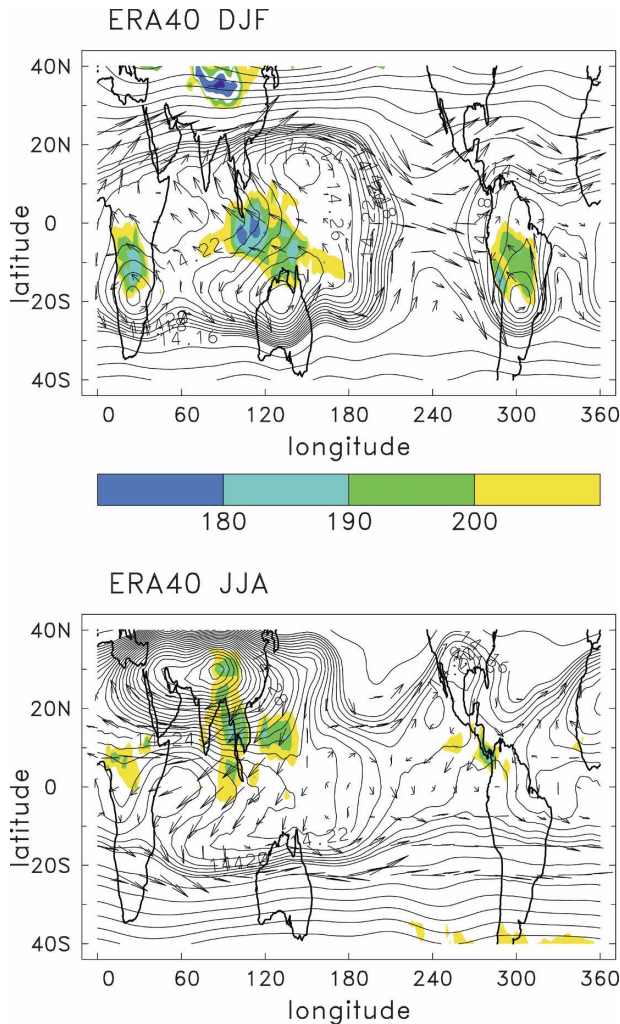


FIG. 9. Vector winds and 200-hPa geopotential height (contours) in the tropics, derived from climatological ERA-40 data for (a) DJF and (b) JJA. The colored contours indicate climatological OLR as a proxy for deep convection.

higher in altitude than those during JJA. This is seen more clearly in Fig. 10, which shows the seasonal cycle of tropical average  $u'v'$  ( $10^\circ\text{N}$ – $10^\circ\text{S}$ ). This clearly shows that the (southward) eddy fluxes during DJF are stronger and extend to a higher altitude than the (northward) fluxes in JJA; in particular, note that the DJF fluxes extend above 100 hPa. This is important because it results in substantially larger subtropical EP flux convergence at and above 100 hPa, and therefore a larger  $\langle \bar{w}_m^* \rangle$ , during DJF. We speculate that the deeper extension of the tropical circulation during DJF is due to the strength of the underlying tropical convection, as discussed further below.

Figure 11 shows the climatological latitude–month structure of  $\overline{u'v'} \cos(\phi)$ —which is proportional to the horizontal EP flux vector, Eq. (4a)—at 100 hPa, illus-

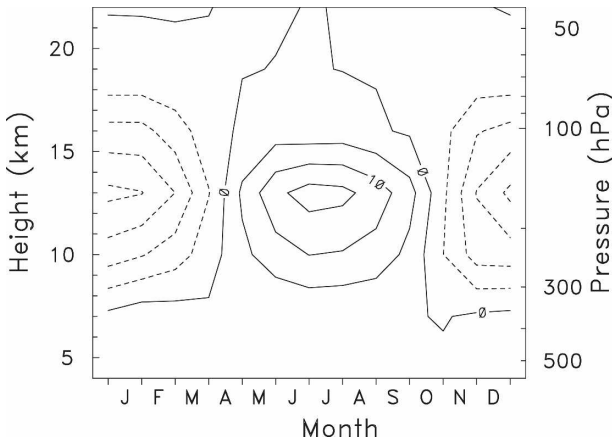


FIG. 10. Height-time section of climatological zonal mean northward eddy momentum flux  $\overline{u'v'}$  averaged over  $10^{\circ}\text{N}$ – $10^{\circ}\text{S}$ , based on NCEP data. Contour interval is  $5 \text{ m}^2 \text{ s}^{-2}$ .

trating the contribution of extratropical and tropical wave forcing in the subtropics. This figure is based on NCEP data, which has somewhat stronger eddy momentum fluxes at 100 hPa compared to ERA-40 data (as can be inferred from Fig. 6), although the overall patterns are very similar. Figure 12 shows a further decomposition of these fluxes into stationary (monthly mean) and transient eddies. In the extratropics there are poleward fluxes in both hemispheres over  $\sim 20^{\circ}$ – $50^{\circ}$ , associated primarily with transient eddies (zonal waves 4–6) in the SH, and approximately equal shares of stationary and transient eddies (planetary-scale zonal waves 1–3) in the NH. There is a relatively strong seasonal cycle to the extratropical  $\overline{u'v'}$  in the NH (maximum in winter, for both the stationary and transient

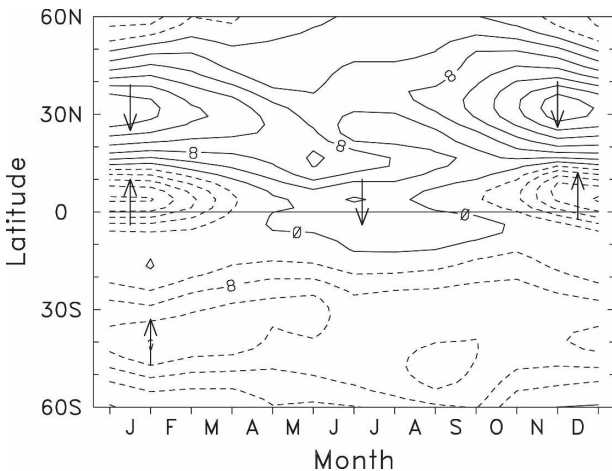


FIG. 11. Latitude-time section of climatological  $\overline{u'v'} \cos(\text{latitude})$  [proportional to the horizontal EP flux vector, Eq. (4a)] at 100 hPa, based on NCEP data. Arrows denote the direction of the associated EP flux. Contour interval is  $4 \text{ m}^2 \text{ s}^{-2}$ .

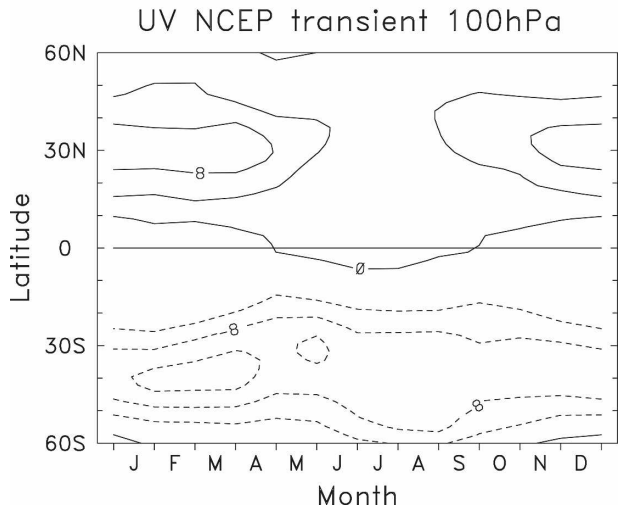
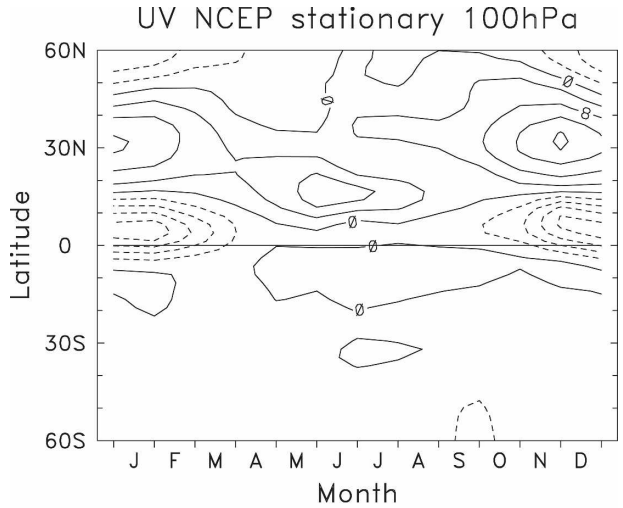


FIG. 12. Latitude-time sections of climatological  $\overline{u'v'} \cos(\text{latitude})$  at 100 hPa (as in Fig. 11), but separated according to (a) stationary and (b) transient eddies. Contour interval in (a) and (b) is  $4 \text{ m}^2 \text{ s}^{-2}$ .

waves), whereas there is weak seasonality in SH extratropical  $\overline{u'v'}$ . The tropical wave fluxes are distinctive in Figs. 11–12, with maximum southward fluxes during  $\sim$ November–March (and northward fluxes during May–August, which do not quite extend to 100 hPa; Fig. 10). The tropical  $\overline{u'v'}$  are primarily associated with stationary (planetary scale) waves (Fig. 12a) because the fluxes occur mainly in the western Pacific region, linked with the strongest convection (Fig. 9). These results show that the maximum in 100-hPa subtropical EP flux convergence during NH winter (and the associated maximum in tropical upwelling seen in Fig. 5) results from the combined effects of enhanced NH extratropical fluxes coupled with the tropical planetary waves (which extend above 100 hPa during this season).

#### 4. Summary and discussion

Upwelling in the tropical lower stratosphere is a dynamically forced phenomenon, associated with wave-induced angular momentum forcing in the subtropics of both hemispheres. We have used ERA-40 and NCEP reanalysis data to calculate the climatological seasonal cycle of upwelling in the UTLS region derived from momentum balance (the “downward control” of Haynes et al. 1991). The resulting estimates of  $\langle \bar{w}_m^* \rangle$  in the deep tropics (15°N–15°S) derived from ERA-40 and NCEP circulation statistics are in reasonable agreement with (independent) thermodynamic estimates  $\langle \bar{w}_\zeta^* \rangle$  at 100 hPa and also with the vertical velocity in ERA-40 reanalysis over the altitude range 10–18 km. There is less agreement for the vertical velocity estimates for the latitude band 25°N–25°S because of substantial differences over 15°–25°N and °S. One possible reason for these differences could be wave forcing associated with gravity waves that are unresolved in the large-scale reanalysis datasets, and in particular wave drag that may occur on top of the subtropical jets (e.g., McFarlane 1987). We have used results from the NCAR WACCM model to demonstrate that such gravity wave drag can lead to enhanced subtropical upwelling (effectively expanding the width of the stratospheric upwelling region); the absence of such wave forcing in large-scale reanalyses is one probable cause of the underestimate of  $\langle \bar{w}_m^* \rangle$  for the latitude bands 15°–25°N and °S (Figs. 2–3). For the deep tropics (15°N–15°S) at 100 hPa, the  $\langle \bar{w}_m^* \rangle$  upwelling estimates show good agreement for the amplitude and phase of the seasonal cycle in upwelling (Fig. 2a). For altitudes above 100 hPa, values of  $\langle \bar{w}_m^* \rangle$  derived from the reanalyses in the deep tropics are smaller than the thermodynamic estimate  $\langle \bar{w}_\zeta^* \rangle$ , although the latter may be overestimated in the calculations here because of the neglect of cloud effects (Yang et al. 2008).

For the latitude band 15°N–15°S, the momentum balance  $\langle \bar{w}_m^* \rangle$  and ERA-40 vertical velocity  $\langle \bar{w}^* \rangle$  (Fig. 5) both show continuous upwelling from 10–20 km (decreasing with altitude up to the lower stratosphere). This suggests that, in a zonal mean sense, there is continual upward transport across the tropical tropopause layer (TTL). This structure can be contrasted with the “clear sky” radiative picture of the TTL region, with a zero radiative heating level at ~15 km separating stratospheric upwelling and upper tropospheric downwelling (Folkins et al. 1999; Gettelman and Forster 2002). These very different vertical structures can be reconciled by a large upward mass flux in the upper troposphere within cloudy regions (which cover only ~10%–20% of the deep tropics), which is in the aggre-

gate larger than the slow clear-sky downwelling (so that the zonal mean is upward at all altitudes). This behavior is consistent with the analyses of Dima and Wallace (2007; see their Fig. 5), although the detailed thermodynamic and radiative balances in the TTL upwelling regions above deep convection remain poorly understood.

The overall realistic behavior of  $\langle \bar{w}_m^* \rangle$  allows analysis of the detailed forcing mechanisms for tropical upwelling, specifically the terms contributing to subtropical EP flux divergence maxima. The results show that horizontal eddy momentum flux convergences are the main contribution to  $\langle \bar{w}_m^* \rangle$  at 100 hPa (Fig. 6) and primarily force the large seasonal cycle. The dominant role of the horizontal momentum flux (horizontal EP flux) in the subtropics for tropical upwelling is somewhat different from the concept that the vertical EP flux in extratropics primarily drives the Brewer–Dobson circulation (Yulaeva et al. 1994; Holton et al. 1995), although the subtropical and extratropical wave forcing are clearly linked. Inspection of EP flux diagrams (Figs. 7–8) show that there are two main sources of subtropical momentum flux convergence, namely midlatitude eddy fluxes and equatorial planetary waves associated with climatological deep convection. At 100 hPa, the extratropical eddy fluxes in the NH are associated with both stationary and transient planetary-scale eddies (zonal waves 1–3), whereas in the SH fluxes are mainly due to transient medium-scale waves (zonal waves 4–6, associated with baroclinic eddies). There is a seasonal maximum to the 100-hPa extratropical NH forcing in winter, but weaker extratropical seasonality in the SH (Fig. 12).

A further comment can be made regarding the altitude at which the driving of the tropical upwelling takes place. As seen in Figs. 8–9, the subtropical EP flux divergence maxima peak in the upper troposphere and decrease with height in the lower stratosphere. This fact, combined with the density weighting for the downward control calculation [Eq. (2)], shows that the upwelling near and above the tropopause is forced near that level. This result can be quantified by limiting the upper level for the integration in (2); such calculations show that for the 100-hPa upwelling over 15°N–15°S (Fig. 2a), 87% of the annual average  $\langle \bar{w}_m^* \rangle$  results for the forcing integrated to 50 hPa (compared to the vertical integral to 1 hPa, using ERA-40 data). Thus, the main driving of the tropical upwelling (and the seasonal cycle) occurs in the UTLS region itself, and there is not an appreciable component from higher altitudes.

The equatorial planetary wave eddy momentum fluxes have a distinctive space–time signature because they are confined primarily to latitudes ~15°N–15°S

and exhibit a seasonally reversing polarity (southward fluxes during NH winter and northward in SH winter). This seasonality is a response to latitudinal movement of tropical convective forcing, and these eddy fluxes are an integral part of the momentum balance with the seasonal Hadley circulation (as discussed by Dima et al. 2005). We note that the importance of equatorial waves for lower stratosphere upwelling has been discussed by Boehm and Lee (2003), Kerr-Munslow and Norton (2006), and Norton (2006), although the details are somewhat different in our analyses. A key feature of the equatorial planetary waves is that the associated eddy momentum fluxes appear to extend to somewhat higher altitudes (above 100 hPa) during NH winter (Fig. 10); in particular, the circulation reaches across 100 hPa in NH winter but not NH summer. These low-latitude momentum fluxes are in balance with the near-equatorial mean meridional flow associated with the Hadley circulation (Dima et al. 2005), so that the convectively forced Hadley circulation appears to extend to higher altitude (across 100 hPa) during NH winter. This seasonal cycle, combined with the seasonal maximum of the NH extratropical fluxes, contributes to the maximum in subtropical wave driving and associated tropical upwelling across 100 hPa during NH winter.

The deeper extension of the tropical planetary waves and Hadley circulation during NH winter has not been noted previously, although it is evident in the results of Dima et al. (2005). We hypothesize that it may be related to the intensity of underlying deep convection near the equator (and associated convective heat release). Figure 13 shows a longitude–month climatology of OLR over 10°N–10°S as a proxy for the intensity of deep convection. Over the western Pacific region there is a substantial seasonal cycle in the deepest convection (low OLR), with a relative maximum during ~November–March. During NH summer the climatological convection is slightly weaker, and it is also situated farther away from the equator (over 10°–20°N, as in Fig. 9b). Although the details of coupling among deep convection, latent heat release, and vertical structure of the Hadley circulation (including equatorial planetary waves spanning the tropics) have not been explored, the deeper extension of the circulation during the season of most intense convection may be suggestive of a causal link. We note that the vast majority (99%) of tropical deep convection reaches altitudes of at most 12–14 km (Gettelman et al. 2002; Liu and Zipser 2005), well below both the tropical tropopause (~17 km) and the range of altitudes with the largest temperature seasonal cycle (~17–20 km). Hence, it does not seem likely that there is a strong influence from tropopause temperature on deep convection; instead, it appears that

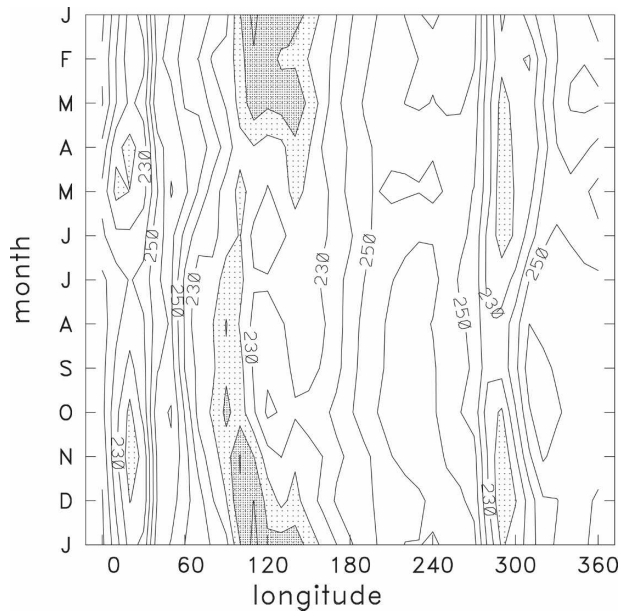


FIG. 13. Longitude–time section of climatological OLR data averaged over 10°N–10°S, used as a proxy for tropical deep convection. Contour interval is  $10 \text{ W m}^{-2}$ ; shaded regions denote the strongest convection (lowest OLR).

convection is the primary driver of this coupling (through the excitation and dissipation of planetary waves).

*Acknowledgments.* We thank several colleagues for discussions during the course of this work and comments on the manuscript, including Andrew Gettelman, Anne Smith, Alan Plumb, Mike Wallace, and Rei Ueyama. This work was partially supported by the NASA ACPMAP Program. The National Center for Atmospheric Research is operated by the University Corporation for Atmospheric Research, under the sponsorship of the National Science Foundation.

#### REFERENCES

- Andrews, D. G., J. R. Holton, and C. B. Leovy, 1987: *Middle Atmosphere Dynamics*. Academic Press, 489 pp.
- Boehm, M. T., and S. Lee, 2003: The implications of tropical Rossby waves for tropical tropopause cirrus formation and for the equatorial upwelling of the Brewer–Dobson circulation. *J. Atmos. Sci.*, **60**, 247–261.
- Brewer, A. W., 1949: Evidence for a world circulation provided by measurements of helium and water vapour distribution in the stratosphere. *Quart. J. Roy. Meteor. Soc.*, **75**, 351–363.
- Butchart, N., and Coauthors, 2006: Simulations of anthropogenic change in the strength of the Brewer–Dobson circulation. *Climate Dyn.*, **27**, 727–741.
- Corti, T., B. P. Luo, Q. Fu, H. Vömel, and T. Peter, 2006: The impact of cirrus clouds on tropical troposphere-to-stratosphere transport. *Atmos. Chem. Phys.*, **6**, 2539–2547.
- Dima, I. M., and J. M. Wallace, 2007: Structure of the annual-

- mean equatorial planetary waves in the ERA-40 reanalyses. *J. Atmos. Sci.*, **64**, 2862–2880.
- , —, and I. Kraucunas, 2005: Tropical zonal momentum balance in the NCEP reanalyses. *J. Atmos. Sci.*, **62**, 2499–2513.
- Dobson, G. M. B., 1956: Origin and distribution of the polyatomic molecules in the atmosphere. *Proc. Roy. Soc. London*, **236A**, 187–193.
- Edmon, H., B. Hoskins, and M. McIntyre, 1980: Eliassen–Palm cross sections for the troposphere. *J. Atmos. Sci.*, **37**, 2600–2616.
- Eluszkiewicz, J., and Coauthors, 1996: Residual circulation in the stratosphere and lower mesosphere as diagnosed from Microwave Limb Sounder data. *J. Atmos. Sci.*, **53**, 217–240.
- Folkens, I., M. Loewenstein, J. Podolske, S. J. Oltmans, and M. Proffitt, 1999: A barrier to vertical mixing at 14 km in the tropics: Evidence from ozonesondes and aircraft measurements. *J. Geophys. Res.*, **104**, 22 095–22 102.
- Fomichev, V. I., A. I. Jonsson, J. de Grandpré, S. R. Beagley, C. McLandress, K. Semeniuk, and T. G. Shepherd, 2007: Response of the middle atmosphere to CO<sub>2</sub> doubling: Results from the Canadian Middle Atmosphere Model. *J. Climate*, **20**, 1121–1144.
- Fueglistaler, S., and Q. Fu, 2006: Impact of clouds on radiative heating rates in the tropical lower stratosphere. *J. Geophys. Res.*, **111**, D23202, doi:10.1029/2006JD007273.
- Garcia, R. R., and W. J. Randel, 2008: Acceleration of the Brewer–Dobson circulation due to increases in greenhouse gases. *J. Atmos. Sci.*, **65**, 2731–2739.
- , D. R. Marsh, D. E. Kinnison, B. A. Boville, and F. Sassi, 2007: Simulation of secular trends in the middle atmosphere, 1950–2003. *J. Geophys. Res.*, **112**, D09301, doi:10.1029/2006JD007485.
- Gottelman, A., and P. M. de F. Forster, 2002: A climatology of the tropical tropopause layer. *J. Meteor. Soc. Japan*, **80**, 911–924.
- , M. L. Salby, and F. Sassi, 2002: Distribution and influence of convection in the tropical tropopause region. *J. Geophys. Res.*, **107**, 4080, doi:10.1029/2001JD001048.
- Gill, A. E., 1980: Some simple solutions for heat-induced tropical circulation. *Quart. J. Roy. Meteor. Soc.*, **106**, 447–462.
- Gille, J. C., L. V. Lyjak, and A. K. Smith, 1987: The global residual mean circulation in the middle atmosphere for the northern winter period. *J. Atmos. Sci.*, **44**, 1437–1452.
- Hall, T. M., and D. W. Waugh, 1997: Tracer transport in the tropical stratosphere due to vertical diffusion and horizontal mixing. *Geophys. Res. Lett.*, **24**, 1383–1386.
- Haynes, P. H., C. J. Marks, M. E. McIntyre, T. G. Shepherd, and K. P. Shine, 1991: On the “downward control” of extratropical diabatic circulations by eddy-induced mean zonal forces. *J. Atmos. Sci.*, **48**, 651–678.
- Holton, J. R., P. Haynes, M. McIntyre, A. Douglass, R. Rood, and L. Pfister, 1995: Stratosphere–troposphere exchange. *Rev. Geophys.*, **33**, 403–439.
- Kalnay, E., and Coauthors, 1996: The NCEP/NCAR 40-Year Reanalysis Project. *Bull. Amer. Meteor. Soc.*, **77**, 437–471.
- Kerr-Munslow, A. M., and W. A. Norton, 2006: Tropical wave driving of the annual cycle in tropical tropopause temperatures. Part I: ECMWF analyses. *J. Atmos. Sci.*, **63**, 1410–1419.
- Liebmann, B., and C. A. Smith, 1996: Description of a complete (interpolated) outgoing longwave radiation dataset. *Bull. Amer. Meteor. Soc.*, **77**, 1275–1277.
- Liu, C., and E. J. Zipser, 2005: Global distribution of convection penetrating the tropical tropopause. *J. Geophys. Res.*, **110**, D23104, doi:10.1029/2005JD006063.
- McFarlane, N. A., 1987: The effect of orographically excited gravity wave drag on the general circulation of the lower stratosphere and troposphere. *J. Atmos. Sci.*, **44**, 1775–1800.
- Mote, P. W., and Coauthors, 1996: An atmospheric tape recorder: The imprint of tropical tropopause temperatures on stratospheric water vapor. *J. Geophys. Res.*, **101**, 3989–4006.
- , T. J. Dunkerton, M. E. McIntyre, E. A. Ray, P. H. Haynes, and J. M. Russell III, 1998: Vertical velocity, vertical diffusion, and dilution by midlatitude air in the tropical lower stratosphere. *J. Geophys. Res.*, **103**, 8651–8666.
- Murgatroyd, R. J., and F. Singleton, 1961: Possible meridional circulations in the stratosphere and mesosphere. *Quart. J. Roy. Meteor. Soc.*, **87**, 125–135.
- Niwano, M., K. Yamazaki, and M. Shiotani, 2003: Seasonal and QBO variations of ascent rate in the tropical lower stratosphere as inferred from UARS HALOE trace gas data. *J. Geophys. Res.*, **108**, 4794, doi:10.1029/2003JD003871.
- Norton, W. A., 2006: Tropical wave driving of the annual cycle in tropical tropopause temperatures. Part II: Model results. *J. Atmos. Sci.*, **63**, 1420–1431.
- Plumb, R. A., and J. Eluszkiewicz, 1999: The Brewer–Dobson circulation: Dynamics of the tropical upwelling. *J. Atmos. Sci.*, **56**, 868–890.
- Randel, W. J., R. R. Garcia, and F. Wu, 2002: Time-dependent upwelling in the tropical lower stratosphere estimated from the zonal-mean momentum budget. *J. Atmos. Sci.*, **59**, 2141–2152.
- , F. Wu, and W. R. Ríos, 2003: Thermal variability of the tropical tropopause region derived from GPS/MET observations. *J. Geophys. Res.*, **108**, 4024, doi:10.1029/2002JD002595.
- , M. Park, F. Wu, and N. Livesey, 2007: A large annual cycle in ozone above the tropical tropopause linked to the Brewer–Dobson circulation. *J. Atmos. Sci.*, **64**, 4479–4488.
- Reed, R. J., and C. L. Vlcek, 1969: The annual temperature variation in the lower tropical stratosphere. *J. Atmos. Sci.*, **26**, 163–167.
- Richter, J. H., F. Sassi, R. R. Garcia, K. Matthes, and C. A. Fischer, 2008: Dynamics of the middle atmosphere as simulated by the Whole Atmosphere Community Climate Model, version 3 (WACCM3). *J. Geophys. Res.*, **113**, D08101, doi:10.1029/2007JD009269.
- Rosenlof, K. H., 1995: Seasonal cycle of the residual mean meridional circulation in the stratosphere. *J. Geophys. Res.*, **100**, 5173–5191.
- Uppala, S. M., and Coauthors, 2005: The ERA-40 re-analysis. *Quart. J. Roy. Meteor. Soc.*, **131**, 2961–3012.
- Wickert, J., and Coauthors, 2001: Atmosphere sounding by GPS radio occultation: First results from CHAMP. *Geophys. Res. Lett.*, **28**, 3263–3266.
- Yang, Q., Q. Fu, J. Austin, A. Gettelman, F. Li, and H. Vomel, 2008: Observationally derived and GCM simulated tropical stratosphere upward mass fluxes. *J. Geophys. Res.*, in press.
- Yulaeva, E., J. R. Holton, and J. M. Wallace, 1994: On the cause of the annual cycle in tropical lower-stratospheric temperatures. *J. Atmos. Sci.*, **51**, 169–174.